Shaping biomimicry: A standardized protocol for soft materials bulk density measurement supporting tissue-like performance

Measurement 268 (2026) 120590

Contents lists available at ScienceDirect

Measurement

journal homepage: www.elsevier.com/locate/measurement

Shaping biomimicry: A standardized protocol for soft materials bulk density measurement supporting tissue-like performance

Sabrina Caria [a,b], Laura Revel [b], Jessica Petiti [b,*], Federico Picollo [a,c], Carla Divieto [b]

[a] Physics Department, University of Turin, Via P. Giuria 1, 10125 Turin, Italy
[b] Division of Advanced Materials Metrology and Life Sciences, Istituto Nazionale di Ricerca Metrologica (INRIM), Strada delle Cacce 91, 10135 Turin, Italy
[c] National Institute for Nuclear Physics (Section of Turin), Via P. Giuria 1, 10125 Turin, Italy

ARTICLE INFO

Keywords:
Bulk density
Phantoms
Biomimicry
Soft materials
Uncertainty
Pycnometer

ABSTRACT

Tissue density is a critical parameter influencing various biological functions, including protein folding and cellular signaling, making accurate measurements essential for advancing our understanding of tissue mechanics and pathology. This work provides a standard operating procedure (SOP) for assessing the bulk density of soft materials using a liquid pycnometer and an analytical balance, along with its validation to ensure precision and reliability. This methodology guarantees precise density evaluations and a rigorous step-by-step procedure for measurement uncertainty estimation. Moreover, the SOP aligns with ASTM F2150-19 standard for biomaterials characterization, which endorses the use of ASTM D792-20 for bulk density measurements, based on the principle of Archimedes. By employing this approach, the study aims to enhance the development of in vitro models for biomedical research, drug testing, and tissue engineering. The SOP allows for bulk density estimation with a relative expanded uncertainty of 3%. Furthermore, it was demonstrated that the material employed for the validation, fibrin gel, is comparable, with a 95% level of confidence, to breast fat, placenta, breast gland, eye (choroid), kidney, liver, heart muscle, pancreas, spleen, diaphragm, eye (ciliary body), muscle, and tongue. Shaping biomimicry: a standardized protocol for soft materials bulk density measurement supporting tissue-like performance.

1. Introduction

Soft matter refers to a class of materials that are easily deformable and exhibit complex rheological properties, often influenced by dynamic fluctuations at the microscopic level. This category includes substances such as liquids [1], liquid crystals, granular materials, gels, foams [2], emulsions, colloids [3], polymers, and various biological materials, e.g. cell membranes, bacterial biofilms, human tissues, which can undergo significant changes in shape and structure in response to external forces. Soft matter is characterized by its ability to flow, stretch, and adapt, making it distinct from hard materials [4,5].

These materials are widely used to create phantoms, such as synthetic models that replicate specific properties of biological tissues, including acoustic, mechanical, thermal, optical, and electrical properties [6]. They serve as analytical standards for linking experimental findings with theoretical models, offering the advantage of providing consistent and customizable tissue-like materials. Tissue phantoms, which possess properties closely resembling those of human tissue, enable accurate simulations for various investigative purposes [7]. In biomedical and biophysical research, they are often used to calibrate and validate clinical instrument prototypes and to optimize the sampling volume of innovative probes [8].

The sensitivity of soft materials to thermal fluctuations and external stimuli, along with their slow response times and long relaxation periods, often results in complex flow behaviors and non-equilibrium states. Unlike hard condensed matter physics, where material properties can often be predicted based on atomic interactions within a regular crystalline lattice, soft matter systems present a more intricate scenario. Their heterogeneous structures, complex interactions across various length scales, and slow dynamics complicate the prediction of material properties. The interplay between interactions and thermal fluctuations can lead to emergent behaviors, such as spontaneous pattern formation and self-assembly, which further complicate the evaluation of soft matter properties [5,9].

Tissue density is a vital parameter that influences various biological functions and processes, making it crucial for advancing our

* Corresponding author.
E-mail address: j.petiti@inrim.it (J. Petiti).

https://doi.org/10.1016/j.measurement.2026.120590
Received 21 October 2025; Received in revised form 12 January 2026; Accepted 24 January 2026
Available online 2 February 2026

understanding of tissue mechanics and pathology [10]. Tissue density is closely linked to buoyancy and the level of crowdedness within biological systems [11], both of which can greatly affect cellular interactions and the overall organization of tissues. Additionally, tissue density is essential for biomolecular condensation [12], impacting critical processes such as protein folding and cellular signaling. Mass density also plays a significant role in the dynamic behavior of biological samples [13], determining how tissues respond to mechanical forces and environmental changes. Moreover, tissue density is key in elastography techniques, such as Brillouin microscopy and transient optical coherence elastography, which use this property to assess mechanical characteristics and gain insights into tissue health and disease states [14,15].

Recognizing the critical role of density in biological tissues, it is essential to thoroughly evaluate the density of materials when developing 3D in vitro models. This evaluation is vital to ensure that the models accurately replicate the physical properties of human tissues, thereby enhancing their relevance and applicability in both research and clinical settings. By achieving a precise match in density, researchers can create more reliable models that better simulate the behavior of actual tissues under various conditions.

This work provides a standard operating procedure (SOP) for evaluating the bulk density of soft materials using a liquid pycnometer and an analytical balance, along with its validation, to ensure reliable and precise measurements. This methodology is often applied in the fields of soil science and geotechnical engineering, where determining bulk density is crucial for understanding soil properties, structure, and behavior. While soil scientists benefit from established protocols [16,17], biomaterials research does not yet adopt standardized SOPs for measuring bulk density and estimating measurement uncertainty, which may hinder comparability across studies [18–20]. The methodology outlined here not only facilitates accurate density measurement but also takes into account the unique characteristics of soft materials, ensuring that the resulting models are both functional and representative of the biological systems they are designed to emulate. Moreover, ASTM F2150-19 [21], the standard guide for the characterization and testing of biomaterial scaffolds used in regenerative medicine and tissue-engineered medical products, recommends assessing bulk density measurements in accordance with the ASTM D792-20 standard [22], which suggests to assess bulk density with methods based on the principle of Archimedes, the same employed in liquid pycnometer measurements. By employing this approach, we aim to advance the development of in vitro models that can significantly contribute to biomedical research, drug testing, and tissue engineering applications.

2. Theoretical background

Bulk density is defined as the ratio of the total mass of a material, including all its components, to the total volume it occupies (bulk volume), which includes both the volume of solid particles and the volume of voids or pores within a sample. This total volume encompasses not only the solid particles but also the void spaces or pores between and within those particles [23–25]. Bulk volume is defined as the total volume occupied by the particles that constitute the material, including their volume, inter-particle void volume, and particles' internal pore volume [26]. Bulk density is typically expressed in grams per cubic centimeter ($g \bullet cm^{-3}$) [27]. By considering both the mass and the volume, bulk density provides valuable insights into the material's compactness and behavior in various applications [23–25].

The measurement of the bulk density quantifies the mass of a material per unit volume.

The general formula for calculating bulk density can be expressed as reported in Eq. (1).

$$\rho_{bulk} = \frac{m}{V} \tag{1}$$

Bulk density varies as a function of both temperature and pressure, and these parameters affect the bulk density value. Different methods and instruments can be used to evaluate the bulk density of liquid and solid materials, such as hydrometers, pycnometers, and digital densimeters [27].

A pycnometer offers several advantages over densimeters and hydrometers, making it a preferred choice for measuring the density of liquids in certain applications. One key advantage is its precision and accuracy. The pycnometer allows for precise control over the volume of liquid being measured, minimizing potential errors associated with buoyancy that can affect the readings of hydrometers and densimeters. Additionally, pycnometers can be used with temperature control, enabling measurements at specific values, which is crucial since density can vary as a function of temperature [28–30].

The pycnometer measures the mass of a known volume directly, simplifying calculations and reducing the potential for error compared to hydrometers, which rely on buoyancy and can be influenced by the shape and size of the liquid container. Furthermore, pycnometers can be used for a wider range of liquids compared with hydrometers or densimeters due to their viscosity or other properties. Overall, the combination of precision, temperature control, direct measurement capabilities, and versatility contributes to the pycnometer's ease of use compared to densimeters and hydrometers [28–30]. A pycnometer is a valuable tool for measuring density, but it also has some disadvantages and limitations. Notably, the experimental process is time-consuming, as the steps of cleaning, filling, and weighing require significant attention and effort. Additionally, the method necessitates a relatively large sample volume, which can be costly. Other limitations belong to the physicochemical properties that the solid must possess for accurate and reliable analysis. Specifically, i) the density of the solid must exceed that of the displaced fluid, ii) the liquid used must not react with, dissolve, or be absorbed by the solid, and iii) the liquid must be capable of completely wetting the surface of the solid [16,17].

A liquid pycnometer (Fig. 1) is primarily designed for measuring the volume and density of liquids, but it can also be adapted for non-destructive density measurement of solid objects. The pycnometer typically consists of a glass flask, referred to as vessel in Fig. 1 and in the following sections, with a close-fitting ground glass stopper that features a capillary hole. This fine hole allows for the release of excess liquid after the pycnometer is filled, ensuring that a specific volume of the measured and/or working liquid, such as water, is obtained with high accuracy [31]. This is achieved by utilizing Archimedes' principle of fluid displacement, which states that an object, whether totally or partially immersed in a fluid, experiences an upward force equal to the weight of the displaced fluid. When measuring the density of a solid using a liquid

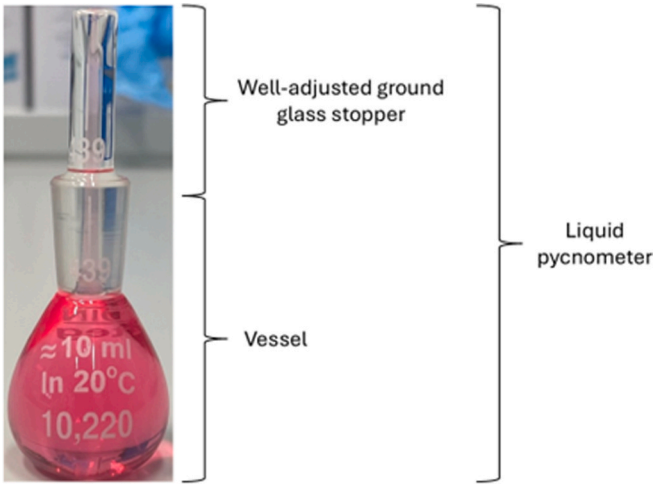

Fig. 1. Image of a liquid pycnometer, featuring labeled graphical representations of its components.

pycnometer, the solid object is submerged in a liquid (usually water) within the pycnometer. The volume of the liquid displaced by the solid can be determined, allowing for the calculation of the solid's volume. This method is effective for obtaining accurate density measurements of solids without altering their physical properties, making the liquid pycnometer a versatile tool in various scientific and industrial applications [32].

3. Standard operating procedure (SOP)

3.1. Materials and equipment

Analytical balance;
Pycnometer with a suitable volume;
Test sample of soft materials;
MilliQ-H_2O (deionized and distilled water with a high purity level that ensures chemically inert behavior);
Appropriate/controlled biological environment (i.e. temperature at 37 °C at 5% CO_2);

3.2. Procedure for evaluating the density of liquids

1. Calibrate and tare the analytical balance before starting measurements;
2. Thoroughly clean the pycnometer with MilliQ-H_2O, rinse it with ethanol (96%), and dry it in an oven at 55 °C for about 30 min;
3. Wait from 30 to 60 min to restore thermal equilibrium between the pycnometer and experimental environment;
4. Measure and record the weight of the empty pycnometer;
5. Remove the pycnometer from the balance plane and tare the instrument again;
6. Repeat points 3 and 4 at least 5 times;
7. Fill the vessel with the liquid to test, insert a well-adjusted ground glass stopper, and let the excess liquid escape;
8. Thoroughly dry the pycnometer external surface with absorbent paper or similar without removing liquid from the capillary (Fig. 2a), ensuring that the liquid reaches the end of the capillary (Fig. 2b) without exceeding it (Fig. 2c);
9. Measure and record the weight of the liquid-filled pycnometer;
10. Remove the pycnometer from the balance plane and tare the instrument again;
11. Record the weight at least 5 times.

3.3. Procedure for evaluating the density of soft matter

1. Calibrate and tare the analytical balance before starting measurements;

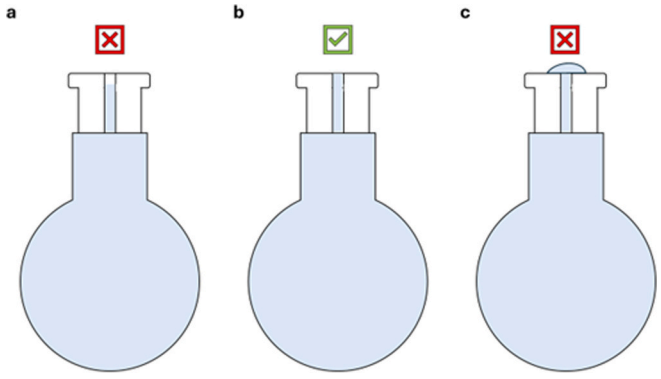

Fig. 2. Graphical explanation of the correct and incorrect way to fill the pycnometer **(a)** incorrect way: the capillary is not completely filled **(b)** correct way: the capillary reaches the end of the capillary **(c)** incorrect way: the liquid exceeds the end of the capillary.

2. Thoroughly clean the pycnometer with MilliQ-H_2O, rinse it with ethanol (96%), and dry it in an oven at 55 °C for about 30 min;
3. Wait from 30 to 60 min to restore thermal equilibrium between the pycnometer and experimental environment;
4. Measure and record the weight of the empty pycnometer;
5. Remove the pycnometer from the balance plane and tare the instrument again;
6. Repeat points 3 and 4 at least 5 times;
7. Fill the vessel with MilliQ-H_2O, insert the well-adjusted ground glass stopper, and let the excess liquid escape;
8. Thoroughly dry the pycnometer without removing MilliQ-H_2O from the capillary, ensuring that the liquid reaches the end of the capillary without exceeding it;
9. Measure and record the weight of the MilliQ-H_2O-filled pycnometer;
10. Remove the pycnometer from the balance plane and tare the instrument again;
11. Repeat points 6, 7, 8, 9, and 10 at least 5 times;
12. Thoroughly dry the pycnometer, insert the soft material into the vessel or synthesize it directly into the vessel to mitigate the risk of damaging and/or losing material, and insert the well-adjusted ground glass stopper;

Note: if the synthesis is performed directly into the vessel, it is important to allow sufficient time for the synthesis to complete before proceeding with the subsequent steps.

13. Measure and record the weight of the soft-material-filled pycnometer;
14. Remove the pycnometer from the balance plane and tare the instrument again;
15. Repeat points 12 and 13 at least 5 times;
16. Fill the vessel containing the soft material with MilliQ-H_2O, insert the well-adjusted ground glass stopper, and let the excess liquid escape;

Note: Porous hydrophilic materials may require gentle agitation and shaking to ensure that MilliQ-H_2O effectively penetrates the pores.

17. Thoroughly dry the pycnometer external surface with absorbent paper or similar without removing MilliQ-H_2O from the capillary, ensuring that the liquid reaches the end of the capillary without exceeding it;
18. Measure and record the weight of the pycnometer filled with soft material and MilliQ-H_2O containing;
19. Remove the pycnometer from the balance plane and tare the instrument again;
20. Repeat points 17 and 18 at least 5 times;

Note: During the measurements, it is important to keep the room temperature as stable as possible and to carry out subsequent measurements quickly in order to minimize the effects induced by time-dependent deformation.

21. Clean and dry the pycnometer;
22. Repeat the entire procedure at least 3 times for each sample to be tested.

3.4. Bulk density calculation

The density of liquids (ρ_L) is determined by measuring the mass of the empty pycnometer (m_1) and the mass of the pycnometer filled with the liquid of interest (m_2). The density is calculated by dividing the difference between the two masses by the known volume of the pycnometer (V_p) as reported in Eq. (2).

$$\rho_L = \frac{m_2 - m_1}{V_p} \quad (2)$$

The density of hydrogels (ρ_S) can be evaluated using the pycnometer by first calculating the specific gravity (*SG*) of the solid, as reported in Eq. (3), and multiplying it by the H_2O density (ρ_{H_2O}) as shown in Eq. (4). A graphical representation of the quantities to evaluate is reported in Fig. 3, and multiplying it by the H_2O density (ρ_{H_2O}).

$$SG = \frac{m_3 - m_1}{(m_3 - m_1) - (m_4 - m_2)} \quad (3)$$

$$\rho_S = \rho_{H_2O} \cdot SG \quad (4)$$

$m_1 = emptypycnometer$

$m_2 = pycnometerfilledwithMilliQ - H_2O$

$m_3 = pycnometercontainingthesolid$

$m_4 = pycnometercontainingthesolidandfilledwithMilliQ{-}H_2O$

3.5. Uncertainty evaluation

3.5.1. For liquids

1. Calculate the mean (M) and standard deviation (SD) of the measured masses m_1 (empty pycnometer) and m_2 (pycnometer filled with liquid).
2. Determine the mass of the liquid with Eq. (5):

$$m_L = m_2 - m_1 \quad (5)$$

3. Propagate the standard uncertainty of the liquid mass according to the Law of Propagation of uncertainty (LPU) [33] using Eq. (6)

$$u(\boldsymbol{m_L}) = \sqrt{\boldsymbol{SD}_{m_2}^2 + \boldsymbol{SD}_{m_1}^2} \quad (6)$$

$SD_{m_2} = standarddeviationofthefilledpycnometer$

$SD_{m_1} = standard\ deviation\ of\ the\ empty\ pycnometer$

4. Use Eq. (7) for the calculation of the density of the liquid:

$$\rho_L = \frac{m_L}{V_p} \quad (7)$$

5. Propagate the standard uncertainty (u) of the density following Eq. (8)

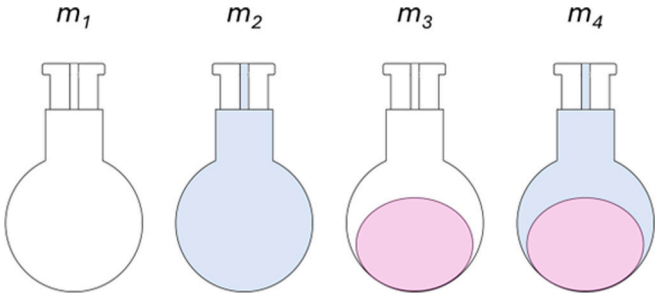

Fig. 3. Graphical representation of , m_1 the empty pycnometer, m_2, the pycnometer filled with H_2O, m_3, the pycnometer with a certain amount of soft material in it, and m_4, the pycnometer filled with the soft material inside and filled with H_2O.

$$u(\rho_L) = \rho_L \sqrt{\left(\frac{u(\boldsymbol{m_L})}{\boldsymbol{m_L}}\right)^2 + \left(\frac{\Delta(\boldsymbol{V_p})}{\boldsymbol{V_p}}\right)^2} \quad (8)$$

$\Delta(\boldsymbol{V_p}) = erroronthevolumeofthepycnometer$

6. Determine the expanded uncertainty at a 95% confidence level ($k = 2$) using Eq. (9)

$$U(\rho_L) = u(\rho_L) \cdot k \quad (9)$$

3.5.2. For soft materials

1. Calculate the uncertainty of the water density (ρ_{H2O}) as explained for liquid samples.
2. Propagate uncertainties for the specific gravity (SG) calculation:

a. Use Eq. (10) for the difference between m_3 and m_1:

$$u(\boldsymbol{m_3} - \boldsymbol{m_1}) = \sqrt{\boldsymbol{SD}_3^2 + \boldsymbol{SD}_{m_1}^2} \quad (10)$$

b. Use Eq. (11) for the difference between m_4 and m_2:

$$u(\boldsymbol{m_4} - \boldsymbol{m_2}) = \sqrt{\boldsymbol{SD}_{m_4}^2 + \boldsymbol{SD}_{m_2}^2} \quad (11)$$

c. Use Eq. (12) for the difference between (m_3-m_1) and (m_3-m_4):

$$u[(\boldsymbol{m_3} - \boldsymbol{m_1}) - (\boldsymbol{m_4} - \boldsymbol{m_2})] = \sqrt{\boldsymbol{u}_{(m_3 - m_1)}^2 + \boldsymbol{u}_{(m_4 - m_2)}^2} \quad (12)$$

d. Use Eq. (13) for the uncertainty of SG:

$$u(SG) = SG \sqrt{\left(\frac{u[(\boldsymbol{m_3} - \boldsymbol{m_1}) - (\boldsymbol{m_4} - \boldsymbol{m_2})]}{[(\boldsymbol{m_3} - \boldsymbol{m_1}) - (\boldsymbol{m_4} - \boldsymbol{m_2})]}\right)^2 + \left(\frac{u(\boldsymbol{m_3} - \boldsymbol{m_1})}{(\boldsymbol{m_3} - \boldsymbol{m_1})}\right)^2} \quad (13)$$

1. Propagate the uncertainty for the density of the soft material following Eq. (14):

$$u(\rho_S) = \rho_S \sqrt{\left(\frac{u(SG)}{\boldsymbol{SG}}\right)^2 + \left(\frac{u(\rho_{H_2O})}{\rho_{H_2O}}\right)^2} \quad (14)$$

2. Calculate the expanded uncertainty for soft materials ($k = 2$) with Eq. (15):

$$U(\rho_S) = u(\rho_S) \cdot k \quad (15)$$

Note: ρ_{H_2O} and $u(\rho_{H_2O})$ correspond to ρ_L and $u(\rho_L)$ calculated for the liquid samples.

4. Application of the SOP: Fibrin gel case study

4.1. Materials & methods

4.1.1. Fibrin gel synthesis protocol

The preparation of fibrin gel was conducted following a protocol developed and refined by our research team. Bovine fibrinogen (Fraction I, type I-S from bovine plasma, Sigma Aldrich, St. Louis, MO, USA) was dissolved in a 0.9% sodium chloride (NaCl) solution (CARLO ERBA

Reagents) at 37 °C to achieve concentrations of either 5 mg/mL or 2.5 mg/mL (Fibrinogen WS). Thrombin powder sourced from bovine plasma (Sigma Aldrich, St. Louis, MO, USA) was reconstituted in MilliQ-H_2O to reach a final concentration of 100 U/mL. After complete dissolution, each solution was sterilized using a 0.22 μm filter. A 50 mM calcium chloride ($CaCl_2$) solution (Sigma Aldrich, USA) was prepared in MilliQ-H_2O and sterilized by autoclaving.

The thrombin solution (100 U/mL), $CaCl_2$ solution, and MilliQ-H_2O were combined in the following ratios: 1:1:0, 1:2:1, and 1:10:9, yielding intermediate thrombin concentrations of 50 U/mL, 25 U/mL, and 5 U/mL, respectively, along with a $CaCl_2$ concentration of 25 mM. To achieve a one-tenth dilution of the thrombin-$CaCl_2$ solution, DMEM culture medium supplemented with 10% heat-inactivated fetal bovine serum (FBS) (Sigma-Aldrich, St. Louis, MO, USA), 2 mM glutamine (Lonza, Basel, Switzerland), and 1% penicillin/streptomycin (Sigma-Aldrich, St. Louis, MO, USA) was added (Thrombin WS).

Fibrin gel was prepared through a sol–gel reaction by combining Fibrinogen WS and Thrombin WS in a 9:11 ratio, resulting in fibrinogen concentrations of 2.25 mg/mL or 1.125 mg/mL, thrombin concentrations of 2.75 U/mL, 1.375 U/mL, and 0.275 U/mL, and a $CaCl_2$ concentration of 1.375 mM. The concentrations used in this study are detailed in Table 1.

4.1.2. Bulk density evaluation

The densities of MilliQ-H_2O and fibrin gel were assessed following the procedure outlined in the SOP. Additionally, the impact of fibrinogen solution aging on fibrin gel density was examined by preparing fibrinogen solutions on day 0 and analyzing fibrin prepared with the same fibrinogen solution on day 0, day 4, and day 7, which corresponds to a fresh, aged for 4 days, and aged for 7 days sample, respectively. The experiment was repeated three times for each combination of fibrinogen and thrombin concentrations tested (Table 1). The influence of different fibrinogen and thrombin concentrations was further studied by measuring fibrin gel density across various concentration combinations, as detailed in Table 3. Each measurement was performed in triplicate for every concentration combination.

4.1.3. Statistical analysis

Statistical analyses were performed using Origin 2022 software (OriginLab Corporation, Northampton, MA, USA). The results are presented as the mean value ± expanded uncertainty (U), to provide a clearer indication of the reliability of the measurements. One-Way ANOVA statistical test was used to study the significance of both the effect of fibrinogen solution aging (density values from technical replicates prepared at day 0, day 3, and day 7 were analyzed as different populations for each fibrinogen-thrombin concentration tested) and different fibrinogen-thrombin combinations on fibrin gel density (all the density values collected for each fibrinogen-thrombin concentration, regardless of the aging state of the fibrinogen solution, represent a distinct population). The fibrin gel density values were compared through a Gaussian test with the tabulated density data of human tissues from the IT'IS database [34] to identify which tissues or organs the fibrin gel could potentially mimic in terms of density.

Table 1
Summary of the reagent concentration used in the work to evaluate the density of fibrin gels.

Sample name	Fibrinogen concentration [mg/mL]	Thrombin concentration [U/mL]	$CaCl_2$ concentration [mM]
F5T50	2.25	2.75	1.375
F5T25	2.25	1.375	1.375
F5T5	2.25	0.275	1.375
F2.5T50	1.125	2.75	1.375
F2.5T25	1.125	1.375	1.375
F2.5T5	1.125	0.275	1.375

Reagent concentrations used for fibrin gel synthesis.

4.2. Results & discussion

The MilliQ-H_2O density results are reported in Fig. 4, while Table 2 shows the measured H_2O density, the reference H_2O density [35], and the room temperature at the time of measurement.

A Gaussian test on the mean values of both the calculated and tabulated MilliQ-H_2O density values was performed, and the result (T = 2.35) indicated a lack of compatibility between these values. Therefore, a correction factor (CF) was introduced to adjust the fibrin gel density values and minimize the influence of temperature on the measurements. The CF was calculated according to Eq. (16).

$$CF = \frac{\rho_{tab}}{\rho_{H_2O}} \tag{16}$$

$$\rho_{tab} = tabulated H_2O density$$

The introduction of a CF in the estimation of ρ_{H_2O} has a direct consequence on the equation used to calculate fibrin gel density. Accordingly, the formula for bulk density calculation was corrected and it is reported in Eq. (17).

$$\rho_s = \rho_{H_2O} \bullet (SG) \bullet (CF) \tag{17}$$

Following this analysis, the equation reported above was used to estimate the fibrin gel density.

Density measurements were performed on fibrin gel synthesized with fibrinogen solution prepared at day 0, and the density was analyzed on day 0 (fresh), day 4 (aged 4), and day 7 (aged 7) using the same fibrinogen solution. For each fibrinogen and thrombin concentration combination, density measurements were performed in triplicate at each aging time. The mean value and the U were calculated for each sample.

The effect of fibrinogen solution aging on different fibrinogen and thrombin solution combinations was investigated. The analysis pointed out that the population means did not differ significantly at the 95% level of confidence, indicating that fibrinogen solution aging did not introduce significant variance in fibrin gel density. Results are shown in Fig. 5 and the corresponding F-statistics and p-values obtained for each population are reported in Table 3.

The influence of different fibrinogen and thrombin solution combinations on fibrin gel density was also investigated. The analysis pointed out that the population means did not differ significantly at the 95% level of confidence, indicating that fibrinogen-thrombin combinations

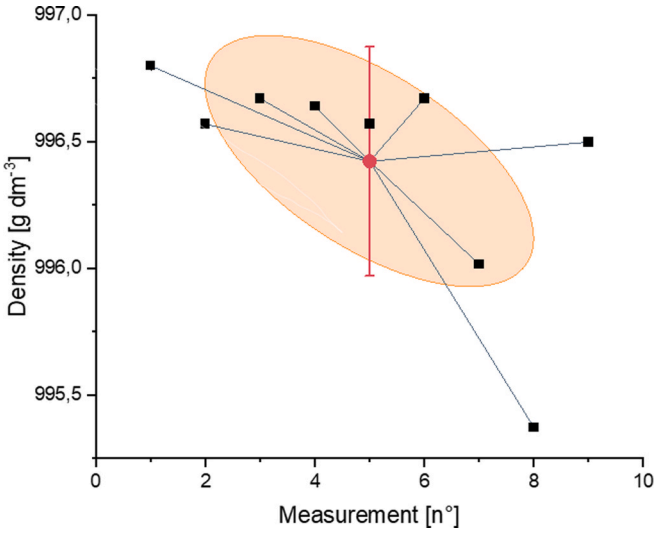

Fig. 4. MilliQ-H_2O density results. Centroid point was evaluated, and the Y error bar corresponds to the SD of all measurements performed.

Table 2
The H_2O density calculated, the H_2O density tabulated, and the temperature of the room at the time of the measurement.

Measure	Temperature [°C]	Calculated H_2O density [g•L^{-1}]	Tabulated H_2O density [g•L^{-1}]
1	23.2	996.799	997.494
2	23.3	996.569	997.470
3	23.3	996.670	997.470
4	23	996.640	997.541
5	23.3	996.644	997.470
6	23.3	996.569	997.470
7	23.1	996.015	997.518
8	23	995.371	997.541
9	23.1	996.498	997.518

Water density values as a function of temperature.

did not introduce significant variance in fibrin gel density. Results are presented in Fig. 6 and the corresponding F-statistics and p-values obtained for each population are reported in Table 4.

The effects of both fibrinogen solution aging and fibrinogen and thrombin solution concentration combinations did not produce a statistically significant variation in fibrin gel density. Therefore, we combined all the density values to calculate the fibrin gels density, expressed as $M \pm U$. The estimated value was 1000 ± 30 g·dm^{-3}.

The relative expanded uncertainty (U%) was calculated according to Eq. (18).

$$U\% = \frac{U \bullet 100}{M} = 3\% \tag{18}$$

Furthermore, the measured fibrin gel density was compared with the density of commercial and non-commercial hydrogels. The density values reported by Chen et al. [36] indicate compatibility between fibrin gel and various non-commercial soft materials, specifically agarose (2% and 3%), alginate (1% and 3%), and gelatin (7% and 10%). Compatibility was also found with polyacrylic acid (PAA) across concentrations of 5% to 20%, polyvinyl alcohol (PVA) at 10%, and polyethylene glycol dimethacrylate (PEDGA) at 15% and 20%. Additionally, fibrin gel shows compatibility with commercial phantoms, including the adult brain phantom (BN-A03) and the adult breast phantom (BT-A02) from True Phantom Solutions, Canada. Finally, fibrin gel density was compared with the density of human tissues present in the IT'IS database using a Gaussian test. The tissue type, estimated density, standard deviation from IT'IS database [34], and the result of the Gaussian tests are reported in Table 5. The Gaussian test results pointed out compatibility, with a 95% level of confidence, between fibrin gel and breast fat, placenta, breast gland, eye (choroid), kidney, liver, heart muscle, pancreas, spleen, diaphragm, eye (ciliary body), muscle, and tongue density. In other words, fibrin gel has the potential to mimic all these human tissues in terms of density.

5. Conclusion

The assessment and calculation of fibrin gel bulk density represents a crucial step in understanding the material's properties and its potential to replicate the typical density of human tissues and organs. The measurement of this parameter not only highlights the similarities and differences between the density of fibrin gel and of various biological tissues but also identifies specific tissues and organs that the biomaterial may effectively mimic in terms of density.

To improve the characterization of soft materials density, we developed detailed, step-by-step instructions (SOP) to facilitate the reliable estimation of bulk density for liquids and soft materials, along with its associated measurement uncertainty. To ensure the accuracy of the measurements, the density of MilliQ-H_2O was first evaluated, and a CF was incorporated into the formula used for calculating fibrin gel density. This rigorous approach enhanced the reliability of the results.

The SOP was then applied to fibrin gel, examining the effects of the

Table 3
F-statistic and p-value obtained through ANOVA statistical test for density values measured at different fibrinogen solution aging stages for each population.

Population	F-statistic	p-value
F5T50	1.42	0.31
F5T25	0.14	0.87
F5T5	0.38	0.70
F2.5T50	1.76	0.25
F2.5T25	1.45	0.31
F2.5T5	0.34	0.72

Statistical results of the effect of fibrinogen solution aging.

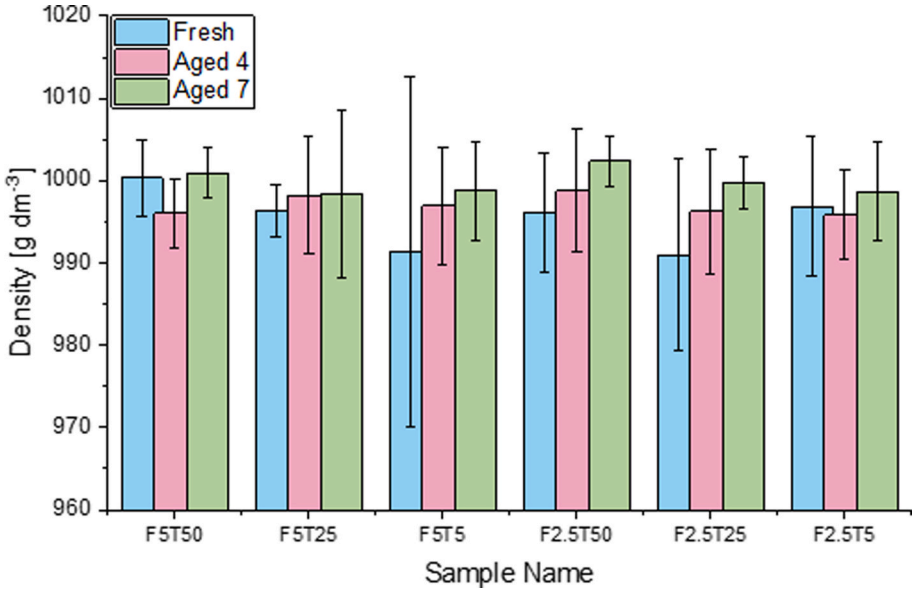

Fig. 5. Results of fibrin gel density measurements analyzing the effects of various fibrinogen and thrombin solution combinations. Each concentration was tested in triplicate for each aging stage of the fibrinogen solution, which was considered non-influential in evaluating the effects of the concentrations. Y error bars represent U.

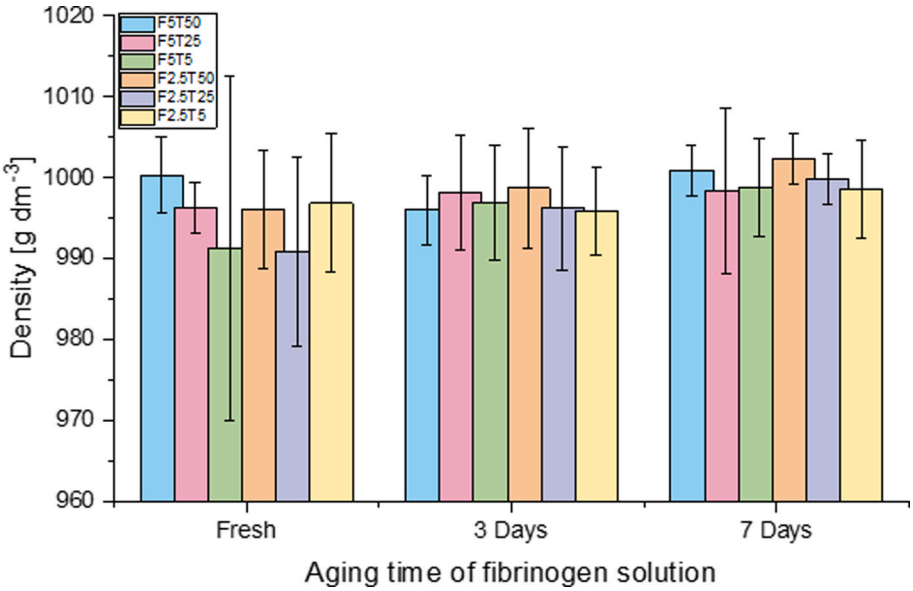

Fig. 6. Results of fibrin gel density measurements analyzing the effects of different fibrinogen solution aging stages. Each aging stage was tested in triplicate for each fibrinogen and thrombin concentration combination, which was considered non-influential in evaluating the aging effect. Y error bars represent U.

Table 4
F-statistic and p-value obtained through ANOVA statistical test for density values measured for different fibrinogen and thrombin solution concentration combinations for each population.

Population	F-statistic	p-value
Fresh	0.48	0.78
Aged 4	0.22	0.94
Aged 7	0.50	0.77

Statistical results of the effect of fibrinogen and thrombin concentrations.

Table 5
Tissues, estimated density, and related SD. Data taken from IT'IS database. Gaussian test result for the comparison between the tissue in question and fibrin gel.

Tissue	Density [g•dm^{-3}]	SD [g•dm^{-3}]	T-test
Lung	394	174	3.4
Breast fat	911	53	1.4
Placenta	1018	33	0.5
Breast gland	1041	45	0.8
Eye (Choroid)	1050	17	1.5
Kidney	1066	56	1.1
Liver	1079	53	1.3
Heart Muscle	1081	36	1.7
Pancreas	1087	59	1.3
Spleen	1089	64	1.3
Diaphragm	1090	52	1.5
Eye (Ciliary Body)	1090	52	1.5
Muscle	1090	52	1.5
Tongue	1090	52	1.5
Skin	1109	14	3.2
Cortical bone	1908	149	6.0
Mandible	1908	133	6.7
Skull	1908	133	6.7
Tooth (Dentine)	2063	79	12.5

Results from comparison between density values of fibrin gel and human tissues.

fibrinogen solution aging, as well as the combinations of fibrinogen and thrombin concentrations. The analyses pointed out the stability of the material, in terms of density, over time and over a range of precursor concentrations for the physical property investigated in this study.

The mean density of the fibrin gel was then compared with established density values of various non-commercial soft materials, commercial phantoms, and human tissues. This comparison revealed that the density of the fibrin gel is comparable to that of several tissues and organs, including breast fat, placenta, breast gland, eye (choroid), kidney, liver, heart muscle, pancreas, spleen, diaphragm, eye (ciliary body), muscle, and tongue.

In conclusion, this SOP provides a useful and reliable tool for an easy and cheap evaluation of the bulk density of liquid and soft material, facilitating the exploitability of this parameter for further research and development of biomaterials as phantoms.

CRediT authorship contribution statement

Sabrina Caria: Writing – original draft, Methodology, Investigation, Formal analysis, Conceptualization. **Laura Revel:** Writing – review & editing, Formal analysis. **Jessica Petiti:** Writing – review & editing, Supervision. **Federico Picollo:** Writing – review & editing. **Carla Divieto:** Writing – review & editing, Supervision, Project administration, Funding acquisition.

Declaration of competing interest

The authors declare that they have no known competing financial interests or personal relationships that could have appeared to influence the work reported in this paper.

Acknowledgements

SC and JP are supported by the GenomeMET Project (grant no.: 22HLT06), funded by European Partnership on Metrology, co-financed by the European Union's Horizon Europe Research and Innovation Programme and by the Participating States.

We thank Dr. Andrea Malengo (Division of Applied metrology and engineering, INRiM) for the willingness to use the pycnometer.

Data availability

Data will be made available on request.

References

[1] M.S. Steinberg, Reconstruction of tissues by dissociated cells, Science 141 (1963) 401–408, https://doi.org/10.1126/science.141.3579.401.

[2] T. Hayashi, R.W. Carthew, Surface mechanics mediate pattern formation in the developing retina, Nature 431 (2004) 647–652, https://doi.org/10.1038/nature02952.

[3] S. Douezan, F. Brochard-Wyart, Dewetting of cellular monolayers, Eur. Phys. J. E 35 (2012) 34, https://doi.org/10.1140/epje/i2012-12034-9.

[4] D. Gonzalez-Rodriguez, K. Guevorkian, S. Douezan, F. Brochard-Wyart, Soft matter models of developing tissues and tumors, Science 338 (2012) 910–917, https://doi.org/10.1126/science.1226418.

[5] V.D. Gucht, Jasper, Grand challenges in soft matter physics, Front. Phys. 6 (2018), https://doi.org/10.3389/fphy.2018.00087.

[6] A. Antoniou, C. Damianou, MR relaxation properties of tissue-mimicking phantoms, Ultrasonics 119 (2022) 106600, https://doi.org/10.1016/j.ultras.2021.106600.

[7] G. Anand, A. Lowe, A. Al-Jumaily, Tissue phantoms to mimic the dielectric properties of human forearm section for multi-frequency bioimpedance analysis at low frequencies, Mater. Sci. Eng. C 96 (2019) 496–508, https://doi.org/10.1016/j.msec.2018.11.080.

[8] F.W.L. Esmonde-White, K.A. Esmonde-White, M.R. Kole, S.A. Goldstein, B. J. Roessler, M.D. Morris, Biomedical tissue phantoms with controlled geometric and optical properties for Raman spectroscopy and tomography, Analyst 136 (2011) 4437–4446, https://doi.org/10.1039/C1AN15429J.

[9] S.R. Nagel, Experimental soft-matter science, Rev. Mod. Phys. 89 (2017), https://doi.org/10.1103/RevModPhys.89.025002.

[10] C. Möckel, T. Beck, S. Kaliman, S. Abuhattum, K. Kim, J. Kolb, D. Wehner, V. Zaburdaev, J. Guck, Estimation of the mass density of biological matter from refractive index measurements, Biophys. Rep. 4 (2024) 100156, https://doi.org/10.1016/j.bpr.2024.100156.

[11] S. Iida, S. Ide, S. Tamura, T. Tani, T. Goto, M. Shribak, K. Maeshima, Orientation-Independent-DIC imaging reveals that a transient rise in depletion force contributes to mitotic chromosome condensation, BioRxiv Prepr. Serv. Biol. (2024), https://doi.org/10.1101/2023.11.11.566679.

[12] J.L. Watson, E. Seinkmane, C.T. Styles, A. Mihut, L.K. Krüger, K.E. McNally, V. J. Planelles-Herrero, M. Dudek, P.M. McCall, S. Barbiero, M. Vanden Oever, S. Y. Peak-Chew, B.T. Porebski, A. Zeng, N.M. Rzechorzek, D.C.S. Wong, A.D. Beale, A. Stangherlin, M. Riggi, J. Iwasa, J. Morf, C. Miliotis, A. Guna, A.J. Inglis, J. Brugués, R.M. Voorhees, J.E. Chambers, Q.-J. Meng, J.S. O'Neill, R.S. Edgar, E. Derivery, Macromolecular condensation buffers intracellular water potential, Nature 623 (2023) 842–852, https://doi.org/10.1038/s41586-023-06626-z.

[13] M. Schürmann, J. Scholze, P. Müller, J. Guck, C.J. Chan, Cell nuclei have lower refractive index and mass density than cytoplasm, J. Biophoton. 9 (2016) 1068–1076, https://doi.org/10.1002/jbio.201500273.

[14] G. Scarcelli, W.J. Polacheck, H.T. Nia, K. Patel, A.J. Grodzinsky, R.D. Kamm, S. H. Yun, Noncontact three-dimensional mapping of intracellular hydromechanical properties by Brillouin microscopy, Nat. Methods 12 (2015) 1132–1134, https://doi.org/10.1038/nmeth.3616.

[15] K.V. Larin, D.D. Sampson, Optical coherence elastography – OCT at work in tissue biomechanics [Invited], Biomed. Opt. Exp. 8 (2017) 1172–1202, https://doi.org/10.1364/BOE.8.001172.

[16] M.A. Helsel, C.F. Ferraris, D. Bentz, Comparative study of methods to measure the density of Cementious powders, J. Test Eval. 44 (2016), https://doi.org/10.1520/JTE20150148.

[17] A. Amoozegar, J.L. Heitman, C.N. Kranz, Comparison of soil particle density determined by a gas pycnometer using helium, nitrogen, and air, Soil Sci. Soc. Am. J. 87 (2023) 1–12, https://doi.org/10.1002/saj2.20476.

[18] K. Mar'ie, I. Lestariningsih, Nurlely, D.S. Soejoko, Phantom design for analysis of CT image quality from Single-source and Dual-source CT scan, J. Phys. Conf. Ser. 1568 (2020) 012019, https://doi.org/10.1088/1742-6596/1568/1/012019.

[19] I. Ozsoykal, A. Yurt, I. Ozsoykal, A. Yurt, Introduction of a novel technique in density-adjusted 3D printing for the manufacture of soft-tissue-equivalent radiological phantoms, Appl. Sci. 14 (2024), https://doi.org/10.3390/app14020509.

[20] A.P. Hariyanto, A.D. Sensusiati, Suprijanto Null, M. Aminah, S.S. Leong, F. Haryanto, K.H. Ng, Endarko Null, Evaluation of physical properties and image quality of a breast tissue phantom with glycerol-enhanced polyvinyl chloride plastisol for ultrasound imaging, Ultrason Seoul Korea 44 (2025) 260–273, https://doi.org/10.14366/usg.24096.

[21] Subcommittee F04.42. Standard Guide for Characterization and Testing of Biomaterial Scaffolds Used in Regenerative Medicine and Tissue-Engineered Medical Products n.d.

[22] Subcommittee D20.70. Standard Test Methods for Density and Specific Gravity (Relative Density) of Plastics by Displacement n.d.

[23] H. Hughes, M.M. Leane, M. Tobyn, J.F. Gamble, S. Munoz, P. Musembi, Development of a material sparing bulk density test comparable to a standard USP method for use in early development of API's, AAPS PharmSciTech 16 (2015) 165–170, https://doi.org/10.1208/s12249-014-0215-7.

[24] J. Cai, Y. He, X. Yu, S.W. Banks, Y. Yang, X. Zhang, Y. Yu, R. Liu, A.V. Bridgwater, Review of physicochemical properties and analytical characterization of lignocellulosic biomass, Renew. Sust. Energy Rev. 76 (2017) 309–322, https://doi.org/10.1016/j.rser.2017.03.072.

[25] A. Shrivastava, 3 - Plastic properties and testing, in: A. Shrivastava (Ed.), Introd. Plast. Eng., William Andrew Publishing, 2018, p. 49–110. doi: 10.1016/B978-0-323-39500-7.00003-4.

[26] N.C. Brady, R.R. Weil, R.R. Weil, The Nature and Properties of Soils, vol. 13, Prentice Hall Upper Saddle River, NJ, 2008.

[27] G.R. Blake, Bulk density, in: Methods Soil Anal., John Wiley & Sons, Ltd, 1965, pp. 374–390, https://doi.org/10.2134/agronmonogr9.1.c30.

[28] Diyari Jabbar, Pycnometric Densitometers, 2025. doi: 10.13140/RG.2.2.11323.32803.

[29] M. Viana, P. Jouannin, C. Pontier, D. Chulia, About pycnometric density measurements, Talanta 57 (2002) 583–593, https://doi.org/10.1016/S0039-9140(02)00058-9.

[30] F. Wardenaar, C.P. Ortega-Santos, K. Vento, S. Olzinski, J. Olig, S. Kavouras, C. Johnston, Reliability of 3 urine specific gravity meters for measuring brix and urine solutions at different temperatures, J. Athl. Train. 56 (2021) 389–395, https://doi.org/10.4085/1062-6050-0142.20.

[31] D. Semnani, 7 - Geometrical characterization of electrospun nanofibers, in: M. Afshari (Ed.), Electrospun Nanofibers, Woodhead Publishing, 2017, p. 151–80. doi: 10.1016/B978-0-08-100907-9.00007-6.

[32] S. Van Vlierberghe, G.-J. Graulus, S. Keshari Samal, I. Van Nieuwenhove, P. Dubruel, 12 - Porous hydrogel biomedical foam scaffolds for tissue repair, in: P.A. Netti (Ed.), Biomed. Foams Tissue Eng. Appl., Woodhead Publishing; 2014, p. 335–90. doi: 10.1533/9780857097033.2.335.

[33] S. Rishi, The law of propagation of uncertainty, in: Pract. Handb. Meas. Uncertain. Faqs Fundam. Metrol., IOP Publishing, 2024, https://doi.org/10.1088/978-0-7503-6462-1ch7.

[34] C. Baumgartner, P.A. Hasgall, F. Di Gennaro, E. Neufeld, B. Lloyd, M. C. Gosselin, D. Payne, A. Klingenböck, N. Kuster. IT'IS Database for Thermal and Electromagnetic Parameters of Biological Tissues, 2025. doi: 10.13099/VIP21000-05-0.

[35] NIST, Thermophysical Properties of Fluid Systems, n.d.

[36] P. Chen, A.M.A.O. Pollet, A. Panfilova, M. Zhou, S. Turco, J.M.J. den Toonder, M. Mischi, Acoustic characterization of tissue-mimicking materials for ultrasound perfusion imaging research, Ultrasound Med. Biol. 48 (2022) 124–142, https://doi.org/10.1016/j.ultrasmedbio.2021.09.004.